MOLECULAR PHYSICS, 1993, VOL. 79, NO. 1, 105–120

The stability of the AB_{13} crystal in a binary hard sphere system

By M. D. ELDRIDGE and P. A. MADDEN
Physical Chemistry Laboratory, Oxford University, South Parks Road, Oxford OX1 3QZ, England

and D. FRENKEL
FOM-Institute for Atomic and Molecular Physics, Kruislaan 407, NL-1098 SJ Amsterdam, The Netherlands

(Received 28 July 1992; accepted 11 September 1992)

A numerical study of the stability of the AB_{13} crystal structure in a mixture of dissimilar hard spheres is reported. This crystal structure has recently been observed by Bartlett and coworkers in experiments on suspensions of colloidal hard-sphere mixtures. We find that, over a range of densities and diameter ratios, the AB_{13} phase is thermodynamically stable both with respect to the fluid mixture and the crystal structures of pure A and pure B. A tentative phase diagram is presented.

1. Introduction

Suspensions of colloidal hard spherical particles play an increasingly important role as model systems that can be used to test theories that have been devised to describe the static and dynamic properties of simple liquids and solids. Experiments on suspensions consisting of spherical particles that interact through a short-range, steeply repulsive potential, have revealed that such simple systems exhibit non-trivial equilibrium [1–4] and non-equilibrium phase behaviour [5–7]. As the ordered phases formed by these colloidal systems have characteristic lattice spacings comparable to the wavelength of visible light, light scattering can be used to probe the structure of colloidal crystals. Monodisperse systems show a first-order phase transition from a disordered fluid phase to a crystalline state with increasing packing fraction. The melting (ϕ_m) and freezing (ϕ_f) packing fractions match very closely those values found from Monte Carlo computer simulations of a hard sphere system [8]. Experimental studies of binary suspensions with varying size ratios have also been undertaken, since the particles can be synthesized with a wide range of diameters [9]. In recent studies of binary mixtures, glass formation, eutectics and binary alloy structures have been reported [7, 10–14].

The present computer simulation study was motivated by the observation of a diffraction pattern attributed to AB_{13} from a solid which crystallized from suspensions with diameter ratios of 0·61 [12] and 0·58 [14]. The AB_{13} structure is equivalent to that of the metallic alloy $NaZn_{13}$. It consists of a simple cubic subcell of the larger component (A). Each cube contains a body-centred B sphere surrounded by twelve B spheres in an icosahedral cluster. The full unit cell consists of eight such subcells with neighbouring icosahedra alternating in orientation by $\pi/2$. The discovery of such a complex crystal (the unit cell contains 112 atoms) in a system with predominantly

short-range, repulsive interactions is, at first sight, surprising. It suggests that the entropy of a dense hard-sphere mixture is maximized by forming a highly ordered crystal structure. However, it is difficult to conclude, on the basis of the available experimental data, that the AB_{13} structure is indeed a thermodynamically stable phase of a binary mixture of hard spherical particles. In particular, the interpretation of the experimental data is complicated by the following factors. First, the colloidal suspensions that are studied experimentally are not truly binary mixtures, as the size distribution of both the large and the small components in the mixture is not infinitely narrow. In addition, the structures formed in these experiments may take weeks or even months to develop. Although this suggests the system has ample time to equilibrate, one cannot rule out the possibility that the crystal structure that has nucleated in these experiments is only metastable. Finally, although colloidal sterically stabilized polymethylmethacrylate (PMMA) particles behave like hard spheres in many respects, their interaction potential is not perfectly hard, nor even purely repulsive. It is conceivable that it is precisely this softness of the intermolecular potential that stabilizes the complex AB_{13} structure. The aim of the computer simulations reported in this paper is to compute the absolute free energy of the AB_{13} structure for a binary mixture of dissimilar hard spheres. Knowledge of this free energy allows us to compare the thermodynamic stability of the AB_{13} phase with respect to other possible phases.

A bidisperse mixture of hard spheres may be expected to form a wider variety of crystal phases than a one-component system. The stability of these crystalline phases depends critically on the diameter ratio, $\alpha = \sigma_B/\sigma_A$, and the mole fractions x_A and x_B of the large and small spheres respectively. There appear to be three distinct classes of crystalline phases exhibited for different ranges of α. Firstly, for the simplest situation when the hard sphere components are of comparable size, we would expect a substitutionally disordered f.c.c. or h.c.p. crystal to be the most stable solid phase. The freezing of binary hard sphere mixtures has been studied recently using approximate density functional theories [15–17] (for a review of the density functional method see [18]). The results of these theories agree well with the recent computer simulations of Kranendonk and Frenkel [19] for size ratios in the range $0{\cdot}85 \leq \alpha \leq 1{\cdot}00$. For diameter ratios greater than $\alpha \approx 0{\cdot}875$, the substitutionally disordered f.c.c. solid is found to be stable, but for $\alpha < 0{\cdot}875$ the hard spheres are no longer miscible in all proportions in the single solid phase. Freezing then occurs into two crystalline phases, one rich in large spheres, the other containing mostly small spheres. The solubility of the large spheres in the crystal of the small spheres becomes very small as the diameter ratio is lowered to below 0·85. The crystal composed mainly of large spheres still contains an appreciable proportion of small spheres. The substitutionally disordered f.c.c. phase is expected to be mechanically unstable for $\alpha < 0{\cdot}85$ [15].

For binary mixtures of very dissimilar diameters, we would expect the formation of interstitial structures to be important. With a close-packed f.c.c. or h.c.p. structure of large spheres at a packing fraction $\eta_A = \phi_{\mathrm{cp}}^{(1)} \approx 0{\cdot}7405$, the small spheres can occupy octahedral holes if they have a diameter ratio of less than 0·414 and the tetrahedral holes can accommodate small spheres with α up to 0·225. The NaCl structure, for example, is generated by filling all of the octahedral holes of an f.c.c. crystal. If the large spheres have a packing fraction equivalent to the melting packing fraction of a monodisperse system, i.e. $\eta_A = \phi_{\mathrm{m}}^{(1)} = 0{\cdot}545$, then the maximum diameter ratio of the interstitial particle is, of course, increased over that of

close packing and for the octahedral site in f.c.c. becomes $\alpha \approx 0{\cdot}57$. Molecular dynamics simulations [20] have shown that for larger diameter ratios than this the resulting interstitial compounds are unstable.

Finally, we have an intermediate range of diameter ratios in which only an ordered non-interstitial binary crystal, with each component on a crystalline sublattice, can be stable. These structures are related to ordered crystalline phases observed in metallic alloys. The stability of several of these binary structures have been explored by use of a space filling principle [21, 22]. This argument is based upon the free volume available to the atoms within the crystal structure. If a given structure exhibits a very high maximum packing fraction then at lower densities the individual atoms will have a large free volume in which to move and hence a high translational entropy. One would expect binary structures capable of exhibiting close-packed densities in excess of the close-packed packing fraction for monodisperse spheres, $\phi_{cp}^{(1)} = 0{\cdot}7405$, to be preferred, especially at high pressures. Murray and Sanders [21] have found two such structures, AB_{13} and AB_2, that have maximum packing fractions greater than that of separate close-packed phases. They point out that if the ideal AB_{13} structure is distorted by reducing the size of the central B in the icosahedron by a small amount the outer B spheres touch at a maximum packing fraction of 0·760. The significance of this is that at overall packing fractions lower than 0·74 one can—by assigning a small free volume to the central particle—achieve a larger free volume for the other twelve particles than they can access in close packed structures. However, for a diameter ratio, $\alpha > 0{\cdot}62$ Murray and Sanders [21] concluded that these crystal structures are unstable with respect to solid state separation.

The AB_{13} and AB_2 crystal structures have been observed experimentally by Pusey and coworkers [7, 12, 14] in a study of the crystallization of mixtures of sterically stabilized polymethylmethacrylate (PMMA) spheres, whose interparticle potential is closely approximated by a hard sphere interaction [23]. For a diameter ratio $\alpha = 0{\cdot}58$, stable AB_{13} and AB_2 were found [14], whereas for $\alpha = 0{\cdot}61$, AB_2 was not observed at all and AB_{13} was found to be metastable [12]. The maximum or close-packed packaging fractions for these two crystal structures are: for $\alpha = 0{\cdot}58$, $\phi_{cp}(AB_2) = 0{\cdot}776$ and $\phi_{cp}(AB_{13}) = 0{\cdot}713$, and for $\alpha = 0{\cdot}61$, $\phi_{cp}(AB_2) = 0{\cdot}750$ and $\phi_{cp}(AB_{13}) = 0{\cdot}685$, for AB_2 and AB_{13} respectively. Thus space filling arguments are in qualitative agreement with the experimental findings. The experimental studies also verified the predictions of the minimal solubility of small spheres in the crystal of large spheres upon phase separation for $\alpha < 0{\cdot}85$.

Bartlett has proposed a simple description for the freezing of binary colloidal hard sphere mixtures. In this picture, the fluid mixture freezes into crystalline solid phases of pure A and pure B [24]. The free energy of a pure hard-sphere solid is known from computer simulations, while a good approximate equation of state exists that allows us to estimate the free energy of the fluid mixture. Bartlett used this information to estimate the phase behaviour of a mixture of dissimilar hard spheres. However, as no information about the free energy of other solid structures (e.g. AB_2 and AB_{13}) was available, Bartlett could not consider the freezing of a hard-sphere mixture into these crystalline phases.

The purpose of the present work is to explore the thermodynamic stability of the AB_{13} crystal by use of free energy calculations. This will enable us to find out if, and when, this more complex solid phase is stable with respect to the phases considered by Bartlett. Section 2 of this paper describes the techniques used in the calculation of

the free energy of the solid phases considered (including AB_{13}) and of the binary fluid. We also consider Bartlett's approach in more detail. In Section 3 we present our phase diagram showing the region of AB_{13} stability and in Section 4 we collect our data in the form of a polynomial fit of the excess free energies of AB_{13} in this region. Finally, a few concluding remarks are made in Section 5.

2. Calculation of free energies

To compare the stability of the different phases that may form in a colloidal suspension we need to know the Helmholtz free energies of all these phases. Below, we indicate how we can estimate this free energy for the fluid and solid phases of interest.

2.1. *The free energy of a binary hard sphere fluid*

The free energy of the fluid phase may be obtained by thermodynamic integration from the dilute gas phase, using the relation:

$$F^{\mathrm{ex}}(\rho) = \int_0^{\rho} \left(\frac{\beta P}{\rho'} - 1 \right) \frac{\mathrm{d}\rho'}{\rho'}, \tag{1}$$

where $F^{\mathrm{ex}}(\rho) \equiv F(\rho) - F^{\mathrm{id}}(\rho)$ is the excess free energy of the fluid at a number density ρ and $F^{\mathrm{id}}(\rho)$ is the free energy of an ideal gas mixture at the same density. Here, and in what follows, we express free energies in units of $k_{\mathrm{B}}T$ per particle. In a binary fluid, composed of N_A large spheres of diameter σ_A and N_B small spheres (σ_B), the partial packing fractions of the two components A and B are given by

$$\eta_i = \frac{\pi}{6} \sigma_i^3 \left(\frac{N_i}{V} \right), \tag{2}$$

where $i = A$ or B. The overall packing fraction, ϕ, is related to the total number density ρ through

$$\phi = \eta_A + \eta_B = \frac{N\pi\sigma_0^3}{6V} = \frac{\pi}{6}\rho\sigma_0^3, \tag{3}$$

where we have defined an average effective hard-sphere diameter σ_0 as

$$\sigma_0^3 = x_A\sigma_A^3 + x_B\sigma_B^3. \tag{4}$$

In order to perform the integration in equation (1) we make use of the semi-empirical expression of Mansoori *et al.* [25] for the pressure, P, of the binary fluid. Mansoori *et al.* approximated the compressibility factor, Z, of a hard sphere fluid mixture by a weighted sum of the compressibility factors obtained from solutions to the Percus–Yevick equations via the compressibility and virial relations [26]

$$Z(\phi) = \tfrac{2}{3} Z_{\mathrm{c}}^{\mathrm{PY}}(\phi) + \tfrac{1}{3} Z_{\mathrm{v}}^{\mathrm{PY}}(\phi). \tag{5}$$

The Mansoori equation of state is written explicitly as

$$\begin{aligned} Z^{\mathrm{Mans}}(\phi) &= \frac{\beta P^{\mathrm{Mans}}}{\rho} = \frac{P^{\mathrm{Mans}} V}{N k_{\mathrm{B}} T} \\ &= \frac{1 + \phi + \phi^2 - 3\phi(y_1 + y_2\phi) - y_3\phi^3}{(1-\phi)^3}, \end{aligned} \tag{6}$$

where

$$y_1(x_A\sigma_A^3 + x_B\sigma_B^3) = x_A x_B(\sigma_A + \sigma_B)(\sigma_A - \sigma_B)^2, \tag{7a}$$

$$y_2(x_A\sigma_A^3 + x_B\sigma_B^3)^2 = x_A x_B \sigma_A \sigma_B (x_A\sigma_A^2 + x_B\sigma_B^2)(\sigma_A - \sigma_B)^2, \tag{7b}$$

$$y_3(x_A\sigma_A^3 + x_B\sigma_B^3)^2 = (x_A\sigma_A^2 + x_B\sigma_B^2)^3. \tag{7c}$$

The accuracy of equation (6) has been tested against molecular dynamics (MD) and Monte Carlo (MC) computer simulations by Jackson *et al.* [27] among others [28]. The Mansoori equation was found to be in good agreement with the numerical results, with significant deviations only occurring for very high densities and/or small diameter ratios. We have also conducted our own MD simulations for a diameter ratio, $\alpha = 0{\cdot}58$, and a composition, $X = x_A = 1/14$. The results are shown in figure 1 and agree well with the Mansoori equation up to very high packing fractions, i.e. $\phi \approx 0{\cdot}55$. Inserting the Mansoori equation into equation (1) yields

$$F^{\mathrm{ex}}(\phi) = \frac{1}{(1-\phi)^2}[\tfrac{3}{2}(1 - y_1) + 3(\tfrac{1}{2} - \phi)y_2 + (\tfrac{3}{2} - 2\phi)y_3] - \ln(1-\phi) + y_3 \ln(1-\phi). \tag{8}$$

In order to get the absolute free energy of the mixture, we now simply add the free energy of an ideal gas mixture at the same density:

$$F^{\mathrm{id}} = -x_A \ln \frac{V}{\Lambda_A^3} - x_B \ln \frac{V}{\Lambda_B^3} + \frac{1}{N}[\ln(N_A!) + \ln(N_B!)], \tag{9}$$

where $\Lambda_A(\Lambda_B)$ is the de Broglie wavelength of species $A(B)$ at temperature T,

$$\Lambda_A = \left(\frac{h^2}{2\pi m_A k_{\mathrm{B}} T}\right)^{1/2}. \tag{10}$$

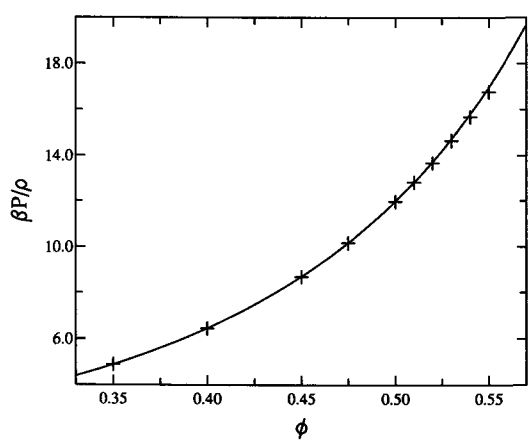

Figure 1. The compression factor, $Z = \beta P/\rho$, obtained from molecular dynamics simulations of a binary hard sphere fluid with composition, $X = 1/14$, and diameter ratio, $\alpha = 0{\cdot}58$ (crosses). These values are compared with those given by the Mansoori equation (full curve).

2.2. *Solid state free energies*

Equation (1) can be used to compute the free energy of any state point that can be reached from the reference state (e.g. the dilute gas), along a *reversible* path. In computer simulations, the freezing transition usually exhibits pronounced hysteresis. As a consequence, equation (1) cannot be used to compute the free energy of a crystalline phase, starting from the gas phase. Instead we have used the lattice-coupling method of Frenkel and Ladd [29] to compute the free energies of the f.c.c. and AB_{13} crystal phases by Monte Carlo simulation. This method is particularly suited for the present study as it allows computation of absolute free energies, thereby allowing the appropriate comparisons of free energies for different phases.

In the Frenkel–Ladd method, a reversible path is constructed from the solid phase that we are interested in, to an Einstein crystal with the same crystallographic structure. This is achieved by slowly turning on harmonic springs binding the particles to their lattice sites, $\mathbf{r}_i^0$. The Hamiltonian for the reference system, i.e. the Einstein crystal, thus becomes

$$\begin{aligned} H(\lambda_A, \lambda_B) &= H_0 + \lambda_A \sum_{i=1}^{N_A} (\mathbf{r}_{i,A} - \mathbf{r}_{i,A}^0)^2 + \lambda_B \sum_{j=1}^{N_B} (\mathbf{r}_{j,B} - \mathbf{r}_{j,B}^0)^2 \\ &= H_0 + \sum_{i=1}^{N} \lambda_i (\mathbf{r}_i - \mathbf{r}_i^0)^2, \end{aligned} \tag{11}$$

for a binary crystal where the large spheres have a coupling constant, λ_A, and the small spheres, λ_B. H_0 is the Hamiltonian for the unperturbed system. In fact, all simulations are carried out on a model system *with fixed centre-of-mass* (see [29]). The latter constraint is imposed most easily if we choose the ratio of the spring constants λ_A and λ_b equal to the ratio of the masses m_A and m_B. It turns out that it is convenient to define an average spring constant, λ_0, *as*

$$\frac{\lambda_0}{m_0} = \frac{\lambda_A}{m_A} = \frac{\lambda_B}{m_B}, \tag{12}$$

where m_0 is the mass of the average particle with diameter σ_0:

$$m_0 = x_A m_A + x_B m_B, \tag{13}$$

$$\Rightarrow \lambda_0 = x_A \lambda_A + x_B \lambda_B. \tag{14}$$

Of course, we are free to choose the masses m_A and m_B. For a classical many-body system, the masses of the particles will not affect the relative stability of the various phases (nor, for that matter, any other static property). The free energy of the system with Hamiltonian, $H(\lambda_A, \lambda_B)$, can now be written

$$\begin{aligned} F(\lambda_A, \lambda_B) &= -k_B T \left\{ \ln \int \ldots \int \exp\left[-\beta H(\lambda_A, \lambda_B)\right] \mathrm{d}\mathbf{q}^N \right\} \\ &= -k_B T \left\{ \ln \int \ldots \int \exp\left[-\beta \left(H_0 + \lambda_0 \sum_i \frac{m_i}{m_0} (\mathbf{r}_i - \mathbf{r}_i^0)^2 \right) \right] \mathrm{d}\mathbf{q}^N \right\}, \end{aligned} \tag{15}$$

and the derivative of the free energy of this system with respect to the average coupling constant, λ_0, becomes

$$\frac{\partial F}{\partial \lambda_0} = \langle V \rangle_{\lambda_0}, \tag{16}$$

where

$$V = \sum_{i=1}^{N} \left(\frac{m_i}{m_0}\right)(\mathbf{r}_i - \mathbf{r}_i^0)^2 = \sum_{i=1}^{N} \left(\frac{\lambda_i}{\lambda_0}\right)(\mathbf{r}_i - \mathbf{r}_i^0)^2. \tag{17}$$

The difference in free energy between the crystal phase under consideration and that with the additional coupling potential, i.e. the interacting Einstein crystal, is therefore

$$\begin{aligned} \Delta F^N &= F^N(\lambda_0 = 0) - F^N(\lambda) \\ &= -\int_0^{\lambda} N\left\langle \frac{\lambda_i}{\lambda_0}(\mathbf{r}_i - \mathbf{r}_i^0)^2 \right\rangle_{\lambda_0} \mathrm{d}\lambda_0. \end{aligned} \tag{18}$$

This free energy difference can conveniently be reformulated to transform the integrand into a smooth function:

$$\Delta F^N = -N \int_{\ln(c)}^{\ln(\lambda+c)} \left[\left\langle \frac{\lambda_i}{\lambda_0}(\mathbf{r}_i - \mathbf{r}_i^0)^2 \right\rangle_{\lambda_0} \times (\lambda_0 + c) \right] \mathrm{d}\ln(\lambda_0 + c), \tag{19}$$

where c is a constant (we used $\ln(c) = 3{\cdot}5$).

In order to compute the integral in (19) and obtain the difference in free energy between our crystal phase and the equivalent non-interacting Einstein crystal, the average $\langle(\lambda_i/\lambda_0)(\mathbf{r}_i - \mathbf{r}_i^0)^2\rangle_{\lambda_0}$ is calculated by Monte Carlo simulation for ten, say, values of λ_0, each determined by a ten-point Gauss–Legendre quadrature weighting on the values of $\ln(\lambda_0 + c)$ in the range: $\ln c \to \ln(\lambda_0 + c)$ [29]. $\lambda_0^{\max}$ is chosen such that the proportion of trial moves that are accepted on the basis of the spring potential energy and *then* cause overlap (i.e. interact) becomes negligible.

All that remains is to derive an expression for the free energy of the non-interacting Einstein crystal with a fixed centre-of-mass.

$$F_{\mathrm{Einst}}^N = -k_{\mathrm{B}} T \ln Q_{\mathrm{Einst}}. \tag{20}$$

The configurational part of the partition for the Einstein crystal with fixed centre-of-mass is

$$Z'_{\mathrm{Einst}} = \int \cdots \int \exp\left[-\beta \sum_{i=1}^{N} \lambda_i (\mathbf{r}_i - \mathbf{r}_i^0)^2\right] \delta\left[\sum_{i=1}^{N} m_i(\mathbf{r}_i - \mathbf{r}_i^0)\right] \mathrm{d}\mathbf{r}_i^N, \tag{21}$$

where the delta function forces the condition of fixed centre-of-mass and can be written

$$\begin{aligned} \delta\left[\sum_{j=1}^{N} \frac{\lambda_j}{\lambda_0}(\mathbf{r}_j - \mathbf{r}_j^0)\right] &= \frac{1}{(2\pi)^3} \int \exp\left\{ i\mathbf{k} \cdot \left[\sum_j \frac{\lambda_j}{\lambda_0}(\mathbf{r}_j - \mathbf{r}_j^0)\right]\right\} \mathrm{d}\mathbf{k} \\ &= \frac{1}{(2\pi)^3} \int \prod_{j=1}^{N} \exp\left[i\mathbf{k} \cdot \frac{\lambda_j}{\lambda_0}(\mathbf{r}_j - \mathbf{r}_j^0)\right] \mathrm{d}\mathbf{k}. \end{aligned} \tag{22}$$

This expression can be used to simplify equation (21):

$$Z'_{\mathrm{Einst}} = \left(\frac{\beta\lambda_0}{\pi N}\right)^{3/2} \left(\frac{\pi}{\beta\lambda_A}\right)^{3N_A/2} \left(\frac{\pi}{\beta\lambda_B}\right)^{3N_B/2}. \tag{23}$$

In our simulations, we compute the free energy difference between an Einstein crystal with fixed centre-of-mass and an AB_{13} hard-sphere crystal, also with fixed

centre-of-mass. The free energy of the unconstrained AB_{13} crystal then follows from the fact that Z_{free}, the configurational part of the partition function of an unconstrained crystal is simply VZ_{CM}, where Z_{CM} denotes the configurational part of the partition function of a (periodic) system with fixed centre-of-mass.

In our calculations, we have not attempted to estimate the dependence of the numerical results on system size. However, as the free energy of the AB_{13} crystal was computed for a system consisting of $N = 896$ particles, we may expect finite-size effects to be small.

Because each free energy requires ten simulations, it is advisable to carry out only a small number of free energy calculations and compute the free energy for other values of the density, ρ, and the size ratio, α, by the appropriate thermodynamic integration procedure. The density dependence of F at constant α can be obtained using equation (1). The compressibility factor is computed in a series of MD simulations of the crystal at different packing fractions, but constant diameter ratio. A

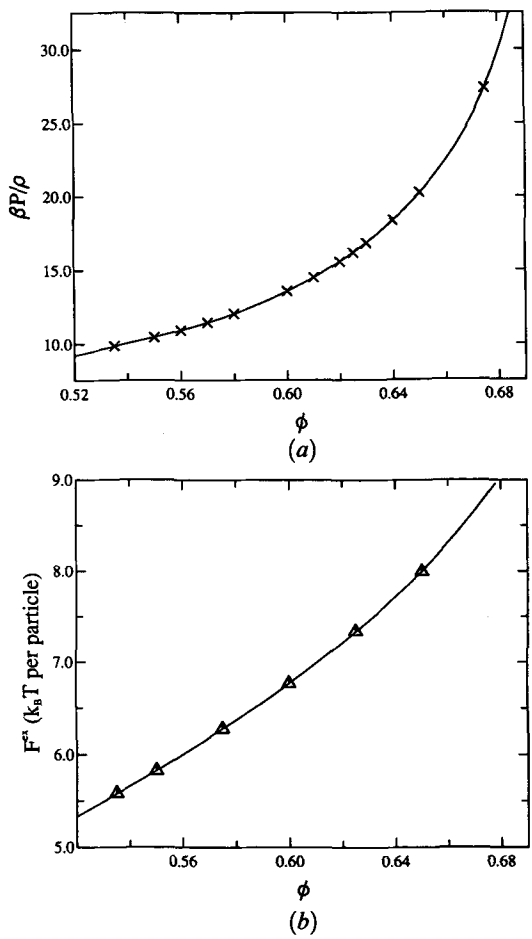

Figure 2. (*a*) The pressure, P, of AB_{13} as a function of the packing fraction, ϕ, for a diameter ratio, $\alpha = 0{\cdot}58$ (crosses) and its polynomial fit (full curve). (*b*) The excess free energies of AB_{13} for $\alpha = 0{\cdot}58$ obtained using the Frenkel–Ladd method (triangles) and the extrapolated free energies (full curve) obtained by integrating the pressure about the point, $\phi = 0{\cdot}60$, as described in the text.

polynomial function is then fitted to these equation-of-state data:

$$Z = \frac{PV}{Nk_BT} = \frac{c_1}{\gamma} + c_2 + c_3\gamma + c_4\gamma^2 + c_5\gamma^3, \tag{24}$$

where

$$\gamma = V^* - 1 = \frac{V}{V_{cp}} - 1 = \frac{\phi_{cp}}{\phi} - 1, \tag{25}$$

and ϕ_{cp} is the close packed or maximum packing fraction. The results of AB_{13} free energies obtained by the Frenkel–Ladd method for a diameter ratio, $\alpha = 0{\cdot}58$, and also those from this integration procedure are shown in figure 2. This figure shows that the integration procedure reproduces the results of the direct free energy calculations to within the statistical accuracy of the latter.

In order to measure the free energy as a function of diameter ratio, at constant packing fraction, we use a technique that has recently been proposed by Kranendonk

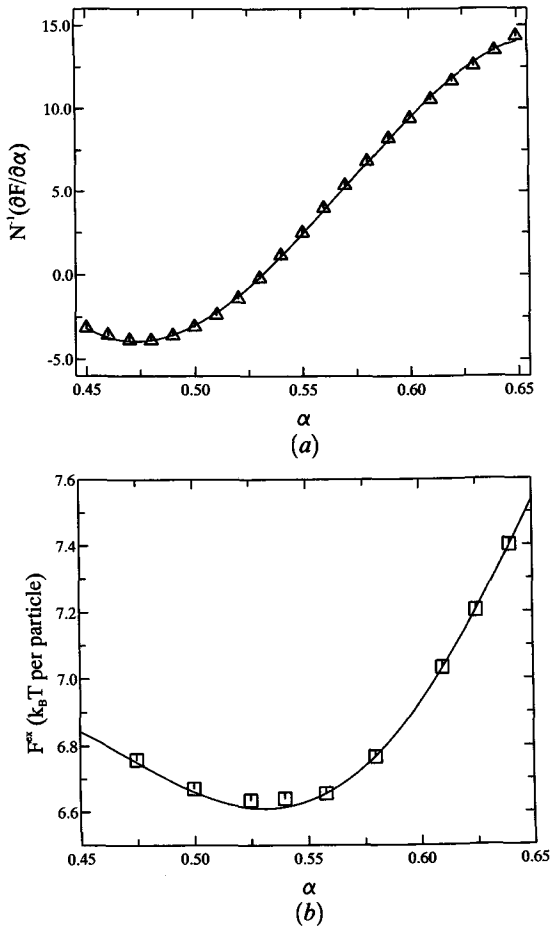

Figure 3. (*a*) The free energy derivative with respect to the diameter ratio, $\partial F/\partial\alpha$, for AB_{13} from MD simulations at $\phi = 0{\cdot}60$ (triangles) and its polynomial fit (full curve). (*b*) the excess free energies of AB_{13} for packing fraction, $\phi = 0{\cdot}60$ obtained using the Frenkel–Ladd method (boxes) and the extrapolated free energies (full curve) obtained by integrating $\partial F/\partial\alpha$ about the point, $\alpha = 0{\cdot}558$.

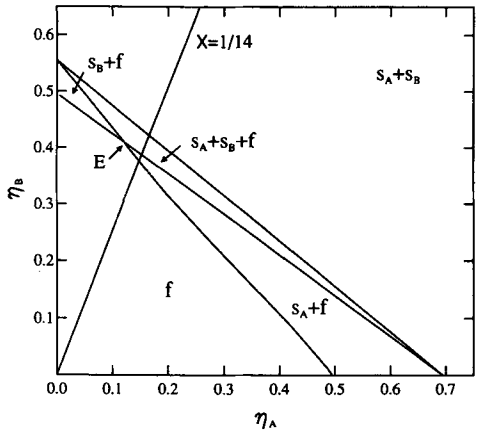

Figure 4. Phase diagram for binary mixtures of hard spheres of diameter ratio, $\alpha = 0{\cdot}58$, arising from the description of Bartlett [24]. $\eta_{A(B)}$ is the partial packing fraction of the large (small) spheres. The labels s_A, s_B and f refer to the solid phase of large spheres (A), the solid phase of small spheres (B) and the fluid phase, respectively. E denotes the eutectic fluid. Also shown is the line of composition, $X = 1/14$, corresponding to AB_{13}.

and Frenkel [30]. In this technique, $\partial F/\partial\alpha$, the free energy change associated with an infinitesimal change in the diameter ratio, at constant overall packing fraction, is computed. In [30] it is shown that this derivative of the free energy is related to the rate of collisional momentum transfer between the particles:

$$\frac{1}{N}\left(\frac{\partial F}{\partial \alpha}\right)_{NVE} = \left(\frac{\sigma_0}{2}\right)\frac{X(1-X)}{[(1-X)\alpha^3 + X]^{4/3}}(\langle f_S^{\mathrm{rad}}\rangle_{NVE} - \alpha^2\langle f_L^{\mathrm{rad}}\rangle_{NVE}). \tag{26}$$

Here, $f_{S(L)}^{\mathrm{rad}}$ is the average radial force exerted on a small (large) particle, which is easily sampled within a molecular dynamics simulation. Again $\partial F/\partial\alpha$ is computed for several different values of α in the range required, at constant ϕ, a polynomial is fitted in α and integrated to obtain the free energy difference. In figure 3 the results obtained using this procedure are compared with the results of

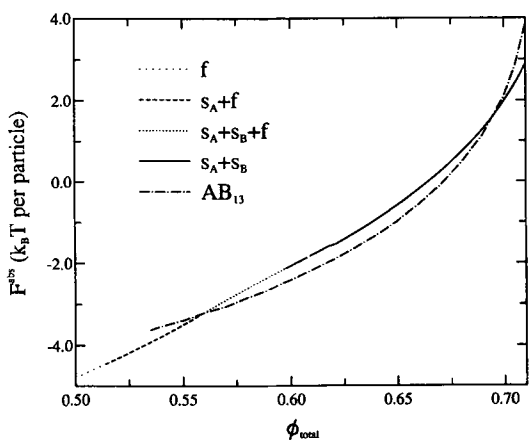

Figure 5. Absolute free energies of AB_{13} (dot–dash curve) and the phases arising from the Bartlett approach [24] for a diameter ratio, $\alpha = 0{\cdot}525$. These phases are fluid (widely-spaced dotted curve), solid A + fluid (dashed curve), solid A + solid B + fluid (closely-spaced dotted curve) and solid A + solid B (full curve).

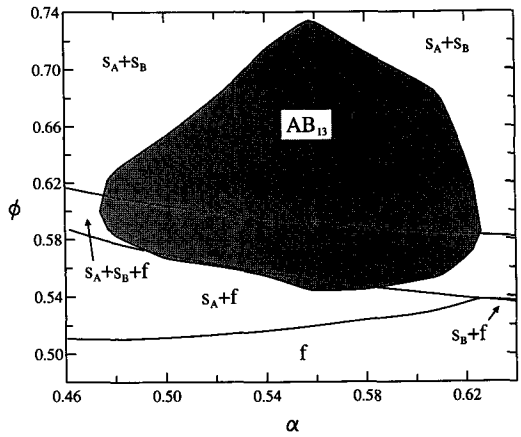

Figure 6. Phase diagram showing the region (shaded) of stability of AB_{13} over the phases arising from the description of Bartlett [24].

direct free energy calculations for diameter ratios in the range $\alpha = 0{\cdot}45 - 0{\cdot}70$ at $\phi = 0{\cdot}60$.

3. Phase diagram for AB_{13}

The central question that we wish to answer in this paper is whether the AB_{13} phase can be more stable than the fluid mixture and the crystalline phases of the pure components. Following Bartlett, we estimate the free energy of the fluid mixture, using the Mansoori equation of state (see Section 2.1.). Bartlett used the parametrization by Alder *et al.* [31] for the equation of state of a f.c.c. hard-sphere crystal based on molecular dynamics calculations:

$$\frac{P_s V_s}{N_i k_B T} = \frac{3}{V^* - 1} + 2{\cdot}566 + 0{\cdot}55(V^* - 1) - 1{\cdot}19(V^* - 1)^2 + 5{\cdot}95(V^* - 1)^3, \quad (27)$$

where the reduced volume, $V^* = (V_s/V_{cp})$. We have performed several MD simulations for the pure component f.c.c. phase which confirm the validity of this expression and found good agreement over the entire solid range.

Using the above approximations for the equation of state of the fluid and (pure) solid phases, we can compute a partial phase diagram of the mixture at a given diameter ratio α. A typical example of such a partial phase diagram is shown in figure 4 for a diameter ratio, $\alpha = 0{\cdot}58$. In this figure, we have indicated the line of constant composition, $X = 1/14$, which corresponds to the AB_{13} structure. If we prepare a system with this overall composition, we should compare the free energy of the AB_{13} structure with the free energies of the fluid mixture (f), the fluid coexisting with solid A ($s_A + f$), the eutectic state where solid A and B coexist with the fluid ($s_A + s_B + f$) and the state in which the system has separated into pure solid A and solid B ($s_A + s_B$). In figure 5 we show, for $\alpha = 0{\cdot}525$, the free energies of the most stable phases along the line $X = 1/14$. The figure shows that, for packing fractions, $0{\cdot}560 < \phi < 0{\cdot}687$, the AB_{13} is more stable than either the fluid mixture or the pure solid phases (the figure for $\alpha = 0{\cdot}58$ is similar but because AB_{13} has a greater range of stability at $\alpha = 0{\cdot}58$ it does not show as clearly the cross-over, at high packing fraction, to favoured stability of $s_A + s_B$ over AB_{13}).

In figure 6 we compare the stability of the AB_{13} phase with the fluid mixture and

the pure solid phases, for a range of diameter ratios, with composition $X = 1/14$. This phase diagram shows the phase region (shaded) of thermodynamic stability of AB_{13} over these simpler phases. This phase behaviour seems, at a qualitative level, to be in good agreement with Bartlett *et al.*'s findings [12, 14]. In particular, in a solution of overall mole fraction, $X = 0{\cdot}057$, at a diameter ratio of 0·61, they found an AB_{13} crystal coexisting with a binary fluid and solid B at an overall packing fraction of 0·535 but no AB_{13} at $\phi = 0{\cdot}511$ and $\phi = 0{\cdot}553$. This is consistent with the behaviour suggested by figure 6 where $\alpha \approx 0{\cdot}62$ is seen to mark the upper limit of stability of AB_{13}. More recently, AB_{13} has been found over a wider composition range with $\alpha = 0{\cdot}58$.

We find that for $\alpha > 0{\cdot}62$, the AB_{13} structure is less stable than a state in which crystals of pure A and pure B have phase separated. This finding is in agreement with the analysis of Murray and Sanders [21]. This suggests that simple packing effects dominate the stability of these hard-sphere crystals. Further evidence for this conclusion comes from the fact that the range of stability of the AB_{13} structure is largest for the diameter ratio that yields the highest close-packing density for AB_{13}, i.e. $\alpha = 0{\cdot}558$.

The space-filling curves of Murray and Sanders show another peak in the close-packing volume fraction at $\alpha = 0{\cdot}303$. However, we have performed some MD simulations in which the AB_{13} structure was found to be unstable at this diameter ratio. While the large spheres (A) kept their simple cubic form intact, the small spheres (B) became delocalized with no icosahedral structure.

Figure 6 also suggests that stable AB_{13} structures with diameter ratios as small as 0·48 could occur. However, for these more extreme diameter ratios the reliability of the Mansoori equation of state of the fluid becomes questionable. There are other reasons why the phase diagram shown in figure 6 is only tentative. First of all, another phase, for example AB_2, may be more stable than AB_{13} for part or all of the shaded region in the figure. In that case, the AB_2 phase would eclipse the AB_{13} phase. Secondly, the melting line was computed using the Mansoori equation to estimate the free energy of the fluid. However, the estimated coexistence density of the binary fluid mixture is estimated to be quite high. So high, in fact, that the Mansoori equation will result in a noticeable over-estimate of the free energy of the fluid. Although this systematic error affects our estimate of the location of the melting line (the fluid should have a slightly greater range of stability), it does not change the estimated location of the solid–solid phase transitions.

4. Fit for the AB_{13} excess free energies

Thus far, we have only considered the phase behaviour of the hard sphere mixture at one fixed overall composition, namely $X = 1/14$, and this was not studied by Pusey and Bartlett. However, our data allow us to compute the phase behaviour as a function of the overall composition of the mixture. To be more precise, we can compute the free energy and pressure of the pure A, pure B and stoichiometric AB_{13} phase as a function of density. If we combine these data with the Mansoori expression for the equation of state of the fluid mixture, we can compute an approximate phase diagram of the mixture, including the AB_{13} phase. Knowledge of this more complete phase diagram would allow us to compare our results with the experiments of Bartlett *et al.* [12] that were all performed at compositions other than $X = 1/14$.

In order to facilitate the calculation of this overall phase diagram, it is convenient to represent our numerical data for the free energy (and, thereby, the equation of state) of the AB_{13} phase in some compact, analytical form. The most natural form for this analytical expression, is a free-volume form, similar to the one used by Alder *et al.* to describe the equation of state of the pure hard-sphere solid (equation (27)). It should be noted, however, that the close-packing density of the AB_{13} phase depends on the diameter ratio, α. In the range of diameter ratios considered here, we can use the expressions that Murray and Sanders [21] derived for the close packing density of the AB_{13} structure for two different ranges of α on either side of $\alpha = 0{\cdot}558$. The two ranges are:

Range 1: $0{\cdot}303 < \alpha \leq 0{\cdot}558$,

$$\phi_{\mathrm{cp},1} = \frac{4\pi(1+13\alpha^3)}{3(\alpha\chi)^3}, \tag{28 a}$$

Range 2: $\alpha > 0{\cdot}558$,

$$\phi_{\mathrm{cp},2} = \frac{\pi}{6}\left(\frac{1+13\alpha^3}{\alpha^3}\right)\left\{2\left[1-\frac{1}{(\epsilon+1)^2}\right]^{1/2}+\left[1-\frac{2}{(\epsilon+1)^2}\right]^{1/2}\right\}^{-3}, \tag{28 b}$$

where χ, ϵ are defined by

$$\chi = \frac{4}{\sqrt{3}(\epsilon+1)}\left[(\epsilon+1)^2-\tfrac{4}{3}\right]^{1/2}+\frac{2}{\alpha\sqrt{3}}\left[(\alpha+1)^2-\frac{16\alpha^2}{3(\epsilon+1)^2}\right]^{1/2}, \tag{29 a}$$

$$\epsilon = \frac{1+2\left(4\sin^2\frac{\pi}{5}-1\right)^{1/2}}{2\sin\frac{\pi}{5}}-1$$

$$= 0{\cdot}9021. \tag{29 b}$$

The dependence of this close-packed density on α is shown in figure 7.

The AB_{13} free energies are presented over the complete region of stability in the form of a contour plot in figure 8. Also shown in this figure is the close-packing density curve. We have fitted these free energies to a function of the form

$$F^{\mathrm{ex}} = \left(p_1 \ln y_1 + \sum_{i=2}^{m} p_i y_1^{i-2}\right)\left(1+\sum_{j=1}^{n} q_j x^j\right) + \left(r_1 \ln y_2 + \sum_{k=2}^{m} r_k y_2^{k-2}\right)\left(1+\sum_{l=1}^{n} s_l x^l\right) \tag{30}$$

where

$$x = \alpha - 0{\cdot}558, \tag{31 a}$$

$$y_1 = \left[\frac{\phi_{\mathrm{cp},1}(\alpha)}{\phi}-1\right], \tag{31 b}$$

$$y_2 = \left[\frac{\phi_{\mathrm{cp},2}(\alpha)}{\phi}-1\right]. \tag{31 c}$$

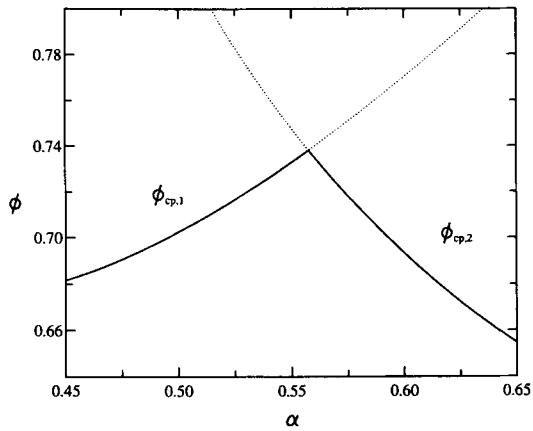

Figure 7. The space-filling curves, i.e. of maximum packing fraction, as a function of α, for AB_{13}.

Note that the space-filling curves, shown in figure 7, are extended beyond their alleged ranges to enable a better fit for the free energy surface. A fit for $m = 4$, $n = 2$ proved sufficient, giving a sum of square differences for a 144-point dataset of 0·1675. The free energy function for this fit is

$$\begin{aligned} F_{\text{fit}}^{\text{ex}} = {} & c_1 + c_2 x + c_3 x^2 + c_4 \ln y_1 + c_5 y_1 + c_6 y_1^2 + c_7 x \ln y_1 + c_8 x y_1 + c_9 x y_1^2 \\ & + c_{10} x^2 \ln y_1 + c_{11} x^2 y_1 + c_{12} x^2 y_1^2 + c_{13} \ln y_2 + c_{14} y_2 + c_{15} y_2^2 + c_{16} x \ln y_2 \\ & + c_{17} x y_2 + c_{18} x y_2^2 + c_{19} x^2 \ln y_2 + c_{20} x^2 y_2 + c_{21} x^2 y_2^2, \end{aligned} \tag{32}$$

and the 21 coefficients, c_i, are given in the table.

5. Discussion

The results we have described indicate a wide range of stability for the AB_{13} phase as a function of size ratio. The domain of stability is centred on the diameter ratio, α, of 0·558, which was shown by Murray and Sanders [21] to be the value at

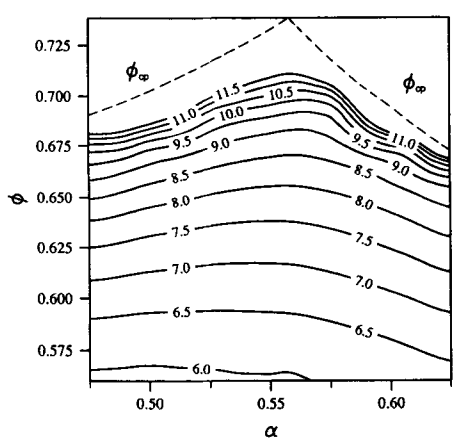

Figure 8. Contour plot for the excess free energies of AB_{13}. The space-filling curve, $\phi_{cp}(\alpha)$, for AB_{13} is also shown.

Table 1. Coefficients for the polynomial fit of the AB_{13} free energy surface.

Coefficient		Basis function
c_1	2·98820	1
c_2	−83·56020	x
c_3	25·09242	x^2
c_4	−2·48057	$\ln y_1$
c_5	13·91956	y_1
c_6	−17·92029	y_1^2
c_7	−22·48370	$x \ln y_1$
c_8	95·00226	xy_1
c_9	−51·44138	xy_1^2
c_{10}	−129·03157	$x^2 \ln y_1$
c_{11}	45·99392	$x^2 y_1$
c_{12}	45·26173	$x^2 y_1^2$
c_{13}	0·02752	$\ln y_2$
c_{14}	−14·18133	y_2
c_{15}	20·13996	y_2^2
c_{16}	−3·57413	$x \ln y_2$
c_{17}	106·88327	xy_2
c_{18}	10·20240	xy_2^2
c_{19}	−27·28941	$x^2 \ln y_2$
c_{20}	−33·43184	$x^2 y_2$
c_{21}	−54·12209	$x^2 y_2^2$

which this crystal would achieve a maximum packing fraction. Murray and Sanders' considerations suggest another domain of stability for this crystal for α close to 0·3, but at these low values of α we find that the small spheres are mobile, even at high packing fraction.

Our results are in qualitative accord with the experimental findings of Bartlett *et al.* [12, 14]. They reported AB_{13} crystals in mixtures with $\alpha = 0{\cdot}58$, which is well within the predicted stability range, and the transient appearance of AB_{13} at $\alpha = 0{\cdot}61$, which is close to the predicted boundary of stability.

The calculations have been made on Parsys Supernode and Meiko i860 parallel computers at the Royal Signals and Radar Establishment (D. R. A. Malvern). We are grateful to Dr J. H. Jefferson for his support and assistance. Calculations have also been made on the Intel i860 hypercube at the Daresbury Laboratory and on IBM RS6000 machines purchased with SERC grant GR/H10276. We would also like to warmly acknowledge numerous helpful discussions with Peter Pusey and Paul Bartlett.

References

[1] Pusey, P. N., and van Megen, W., 1986, *Nature*, **320**, 340.
[2] Pusey, P. N., van Megen, W., Bartlett, P., Ackerson, B. J., Rarity, J. G., and Underwood, S. M., 1989, *Phys. Rev. Lett.*, **63**, 2753.
[3] Pusey, P. N., 1991, *Liquids, Freezing and the Glass Transition*, Les Houches, Session LI, 1989, edited by J. P. Hansen, D. Levesque and J. Zinn-Justin (Amsterdam: Elsevier), pp. 763–942.
[4] van Megen, W., Pusey, P. N., and Bartlett, P., 1990, *Phase Transitions*, **21**, 207.

[5] PUSEY, P. N., and VAN MEGEN, W., 1987, *Phys. Rev. Lett.*, **59**, 2083.
[6] ACKERSON, B. J., and PUSEY, P. N., 1988, *Phys. Rev. Lett.*, **61**, 1033.
[7] PUSEY, P. N., VAN MEGEN, W., UNDERWOOD, S. M., BARTLETT, P., and OTTEWILL, R. H., 1990, *J. Phys.: Condensed Matter*, **2**, SA373.
[8] HOOVER, W. G., and REE, F. H., 1968, *J. chem. Phys.*, **49**, 3609.
[9] ANTL, L., GOODWIN, J. W., HILL, R. D., OTTEWILL, R. H., OWENS, S. M., PAPWORTH, S., and WATERS, J. A., 1986, *Colloid Surf.*, **17**, 67.
[10] YOSHIMURA, S., and HACHISU, S., 1983, *Prog. Colloid Polymer Sci.*, **68**, 59; 1985, *J. Physique*, **46**, C3, 115.
[11] HACHISU, S., and YOSHIMURA, S., 1987, *Physics of Complex and Supermolecular Fluids*, edited by S. A. Safran and N. A. Clark (New York: Wiley).
[12] BARTLETT, P., OTTEWILL, R. H., and PUSEY, P. N., 1990, *J. chem. Phys.*, **93**, 1299.
[13] BARTLETT, P., and OTTEWILL, R. H., 1992, *J. chem. Phys.*, **96**, 3306.
[14] BARTLETT, P., OTTEWILL, R. H., and PUSEY, P. N., 1992, *Phys. Rev. Lett.*, **68**, 3801.
[15] BARRAT, J. L., BAUS, M., and HANSEN, J. P., 1986, *Phys. Rev. Lett.*, **56**, 1063; 1987, *J. Phys.* C, **20**, 1413.
[16] ZENG, X. C., and OXTOBY, D. W., 1990, *J. chem. Phys.*, **93**, 4357.
[17] DENTON, A. R., and ASHCROFT, N. W., 1990, *Phys. Rev.* A, **42**, 7312.
[18] OXTOBY, D. W., 1991, *Liquids, Freezing and the Glass Transition*, Les Houches, Session LI, 1989, edited by J. P. Hansen, D. Levesque and J. Zinn-Justin (Amsterdam: Elsevier), pp. 145–191.
[19] KRANENDONK, W. G. T., and FRENKEL, D., 1991, *Molec. Phys.*, **72**, 679.
[20] ERMAK, D. L., ALDER, B. J., and PRATT, L. R., 1981, *J. phys. Chem.*, **85**, 3221.
[21] MURRAY, M. J., and SANDERS, J. V., 1980, *Phil. Mag.* A, **42**, 721.
[22] PARTHÉ, E., 1961, *Z. Kristallogr.*, **115**, 52.
[23] LIVSEY, I., and OTTEWILL, R. H., 1989, *Colloid Polym. Sci.*, **267**, 421.
[24] BARTLETT, P., 1990, *J. Phys.: Condensed Matter*, **2**, 4979.
[25] MANSOORI, G. A., CARNAHAN, N. F., STARLING, K. E., and LELAND, T. W., 1971, *J. chem. Phys.*, **54**, 1523.
[26] LEBOWITZ, J. L., 1964, *Phys. Rev.* A, **133**, 895.
[27] JACKSON, G., ROWLINSON, J. S., and VAN SWOL, F., 1987, *J. phys. Chem.*, **91**, 4907.
[28] SMITH, E. B., and LEA, K. R., 1963, *Trans. Faraday Soc.*, **59**, 1535; ROTENBERG, A. J., 1965, *J. chem. Phys.*, **43**, 4377; FRIES, P. H., and HANSEN, J. P., 1983, *Molec. Phys.*, **48**, 891; ALDER, B. J., 1964, *J. chem. Phys.*, **40**, 2724.
[29] FRENKEL, D., and LADD, A. J. C., 1984, *J. Chem. Phys.*, **81**, 3188.
[30] KRANENDONK, W. G. T., and FRENKEL, D., 1991, *Molec. Phys.*, **72**, 699.
[31] ALDER, B. J., HOOVER, W. G., and YOUNG, D. A., 1968, *J. chem. Phys.*, **49**, 3688; YOUNG, D. A., and ALDER, B. J., 1979, *Ibid.*, **70**, 473.